Nanoscale

PAPER

View Article Online
View Journal | View Issue

Published on 05 February 2016. Downloaded by National University of Singapore on 12/05/2016 03:40:10.

Cite this: *Nanoscale*, 2016, **8**, 5657

Fano resonant $Ge_2Sb_2Te_5$ nanoparticles realize switchable lateral optical force†

Tun Cao,*[a] Libang Mao,[a] Dongliang Gao,[b] Weiqiang Ding[c] and Cheng-Wei Qiu*[d]

Received 11th December 2015,
Accepted 5th February 2016

DOI: 10.1039/c5nr08804f

www.rsc.org/nanoscale

Sophisticated optical micromanipulation of small biomolecules usually relies on complex light, *e.g.*, structured light, highly non-paraxial light, or chiral light. One emerging technique is to employ chiral light to drive the chiral nanoparticle along the direction perpendicular to the propagation of the light, *i.e.*, the lateral optical force. Here, we theoretically study the lateral optical force exerted by a entirely Gaussian beam. For the very first time we demonstrate that the Fano resonances (FRs) of the $Ge_2Sb_2Te_5$ (GST) phase-change nanoparticles encapsulated with Au shells could enable a conventional Gaussian laser to exert a lateral force on such a dielectric GST nanoparticle, attributed to the strongly asymmetric energy flow around the sphere in the dipole–quadrupole FRs. More interestingly, the direction of this lateral force could be reversible during the state transition (*i.e.*, from amorphous to crystalline). By bonding small biomolecules to the outer surface of the phase-change nanoparticle, the particle behaves as a direction-selective vehicle to transport biomolecules along opposite directions, at pre-assessed states of the $Ge_2Sb_2Te_5$ core correspondingly. Importantly, the origin of the reversal of the lateral optical force is further unveiled by the optical singularity of the Poynting vector. Our mechanism of tailoring the FRs of phase-change nanoparticles, not just limited to GST, may bring a new twist to optical micromanipulation and biomedical applications.

1. Introduction

Optical trapping and the manipulation of objects have been emerging research fields over the last decades.[1–5] Optical force has played a crucial role in various optical manipulation techniques such as optical tweezing, binding and cavity mechanics.[6,7] However, the fundamental mechanism of optical trapping is based on the "optical gradient force" which is proportional to the size of the entity,[8] thus there is a difficulty in trapping small objects such as biomolecules. The biomolecule typically has a preference for a chiral configuration that cannot be superimposed upon its mirror image.[9] Its interaction with circularly polarized light (CPL) enables the efficient recognition of the material's chirality by an opposite handed version of another material.[10] This interaction leads to a methodological approach to distinguish and harness the handedness of an entity under chiral light. Therefore, modern trends entail the manipulation of a chiral nanoparticle (*i.e.*, a biomolecule) along the direction perpendicular to the propagation of the chiral light using the lateral optical force.[11] There have been fascinating developments in sensitive probing[12,13] and the sorting of molecular chirality[14–16] by means of the interaction between nanoparticles and chiral light. However, these chiral sorting strategies for separating two molecules that differ by their handedness are restricted by the requirement of complex light excitation.

More recently, an option based on the coupling between structural chirality and the beam reflected from the substrate surface has been proposed; it induces a lateral optical force that drags helical Au nanoparticles with opposite handedness in opposite directions using a linearly polarized plane wave.[17] This work certainly motivates the development of the practical realization of the optical sorting of nanoparticles owing to the advantage of using simple light.[18–20] Nonetheless, the direction of the sideways force in this system still depends on the handedness of the chiral particle and has to employ a metal or dielectric substrate.

Fano resonance (FR) arises from the coupling between a narrow resonant line width system and a system with a broader resonance.[21,22] Over the past few years, FR has been observed in a number of plasmonic nanostructures[23–28] and

[a]*Department of Biomedical Engineering, Dalian University of Technology, Dalian 116024, China. E-mail: caotun1806@dlut.edu.cn*
[b]*College of Physics, Optoelectronics and Energy & Collaborative Innovation Center of Suzhou Nano Science and Technology, Soochow University, Suzhou 215006, China*
[c]*Department of Physics, Harbin Institute of Technology, Harbin 150001, China*
[d]*Department of Electrical and Computer Engineering, National University of Singapore, 4 Engineering Drive 3, Singapore 117576, Republic of Singapore. E-mail: eleqc@nus.edu.sg*

† Electronic supplementary information (ESI) available: Absorption cross section of the phase-change particles, optimization of the size of the core and shell and dynamical simulation of stability. See DOI: 10.1039/c5nr08804f

Published on 05 February 2016. Downloaded by National University of Singapore on 12/05/2016 03:40:10.

photonic systems.[29] As FR originates from the interference between two or more oscillators, it possesses a narrower line width than the normal dipolar plasmon peak, and hence exhibits a high sensitivity to the changes in the geometry or local environment.[23] Therefore, devices exploiting FR are promising candidates to improve applications such as sensing,[30,31] switching,[32] nanoantennas[33–35] and wave-mixing.[36]

Very recently, a Fano interference-induced force has been proposed to obtain an ultrasensitive size-selective sorting of only several nanometers for achiral particles in the lateral direction under non-chiral light excitation.[37] This has opened a new perspective in the development of a non-chiral separation technique at the molecular scale. Even so, this method is based on the fact that the dipole–quadrupole interference induced force is controlled by the shell thickness of the nanoparticle thus this limits its application in the separation of the same geometric entities with different material properties. It is noteworthy that the core–shell plasmon mode properties can also be dramatically modified by the core and embedding medium permittivities.[38] Drawing on insights from this interesting phenomenon, it would therefore be of great interest to further explore the Fano interference force in a tunable plasmonic core–shell system, where the surface plasmon resonances (SPRs) can be actively tuned by changing the dielectric constant of the core medium.

Our intuitive picture was that the Fano interference optical force may be reversibly tuned, in a manner determined by a switchable shift of the resonant frequency of the core–shell, which can be achieved through a reconfigurable change of the dielectric permittivity of the core. Thereby, this active tuning of the Fano interference force can be applied for the switchable sorting of the same geometric nanoparticles with various material properties.

With this idea in mind, here we report a theoretical study of the ultrafast reversible sorting of phase-change nanoparticles using an actively tuned transverse force under a linearly polarized Gaussian beam excitation. We examine the lateral optical force on an Au nanoshell with a phase-change material (PCM) core of $Ge_2Sb_2Te_5$, which is designated to support the FR caused by a dipole–quadrupole (DQ) interference. It is found that in a single Gaussian light beam, the asymmetric energy distribution around the core–shell at the DQ Fano interference will produce a lateral optical force. The lateral optical force could move nanoparticles with different states of the $Ge_2Sb_2Te_5$ in opposite directions since the DQ-FRs of the particles can be actively tuned by changing the states of the $Ge_2Sb_2Te_5$.

This shows that the Poynting vector (**S**) can provide a clear physical interpretation of the light–matter interaction, where **S** is treated as the energy flow referred to in Poynting's theorem. Nye and Berry first investigated wave front dislocations,[39] and recently, the optical singularity of **S** has been further employed to understand the mechanism of special optical micromanipulation, *e.g.*, tractor beams.[40,41] Importantly, the optical singularity and FR are in fact strongly related since their origin of interference is identical.[42,43] Therefore, the study of the topology of the optical singularity and the trajectory of the energy flux is significantly instructive to understand the origin of the FR induced optical force acting on the particle. Singular points in **S** are normally classified as a sink node, saddle, vortex, and focus.[44] The energy flow changes with the singular point, hence altering the optical force exerted on the particle. Here, we relate the FR induced total lateral force of a Gaussian beam with **S** and explore its fundamental tenet by investigating the optical singularity. We interpret the mechanism of the total lateral force as a consequence of the specific energy flow. Moreover, it shows that the reversal of the total lateral optical force can be achieved by manipulating the distribution of the singular points around the nanoparticles, where the change of the singular points distribution is caused by the switchable phase transition between the amorphous and crystalline states of the $Ge_2Sb_2Te_5$.[45] Such an advantage enables the system to realize the reversible manipulating and sorting of the particles under a single non-chiral light beam. We also reveal that this technique can be utilized to sort the biomolecules that are bonded to the outer surfaces of the phase-change nanoparticles. This work may further promote the development of the existing biomolecule sorting strategies.

Phase change materials (PCMs) have been developed over the years and are used in rewritable DVD technology with optical laser based switching and will be used in the next generation phase change random access memory technology with high speed electronic switching.[46] Particularly, PCM memory operation, based on the reversible switching between amorphous and crystalline states, is generally achieved by electrical Joule heating in phase-change-random access memory (PC-RAM). Thus our proposed $Ge_2Sb_2Te_5$/Au core–shell particles can adapt these approaches to develop a practical, low cost, high speed and switchable optical sorting technology. Finally, it should be noted that $Ge_2Sb_2Te_5$ does not require any energy to maintain the structural state of the material. Therefore, once the phase-change nanoparticle has been switched it will retain its lateral force until it is switched again. This obviously makes the reversible sorting of the particles interesting from a 'green technology' perspective.

2. Results and discussion

2.1 Lateral optical force on phase-change nanoparticles in the focal plane of the Gaussian beam

FR has been observed in core–shell particles due to the interaction between the dipolar and quadrupolar resonances.[23] It has also been shown that FR enhancement can be obtained for the core–shell particles since the dipolar and quadrupolar resonances can be easily tuned by varying the shell's thickness and the core medium,[47] which determines the strength of the coupling between the adjacent plasmon modes of the core–shell. In this context, we envisage the possibility of switchable sorting of core–shell particles using the reversible Fano interference-induced lateral force under a low incident power. Consider the phase-change nanoparticle with a $Ge_2Sb_2Te_5$ core

 This journal is © The Royal Society of Chemistry 2016

Published on 05 February 2016. Downloaded by National University of Singapore on 12/05/2016 03:40:10.

(radius: R_{PCM} = 70 nm) and an Au shell (thickness: T_{Au} = 20 nm) shown in the inset of Fig. 1(d). A more detailed study of the choice of R_{PCM} = 70 nm and T_{Au} = 20 nm is provided in ESI S2.† As a proof-of-concept demonstration for the reversible optical sorting of the target objects, we assume that a biomolecule, polystyrene sulfonate sodium salt (PSS) (thickness T_{PSS} = 1 nm, refractive index n_{PSS} = 1.484), homogeneously surrounds the outer surfaces of the two phase-change nanoparticles with amorphous and crystalline states. The dielectric properties of Au as given by Johnson & Christy are used.[48]

We are interested in the variation of the Fano interference-induced lateral force exerted on the phase-change nanoparticle as $Ge_2Sb_2Te_5$ transits from the amorphous to the crystalline state. The phase-change nanoparticle is normally illuminated by a linearly polarized Gaussian wave and located at $x = w_0/2$ in the Gaussian beam, where w_0 = 500 nm is the beam waist and the incident electric field vector (E) is parallel to the x-axis (see Fig. 1(d)). The environment is water. The incident light power is P_0 = 10 mW. For a phase-change nanoparticle, it is expected that the transverse optical force under a normal inhomogeneous incident beam will push it in the direction determined by the structural phase of $Ge_2Sb_2Te_5$.

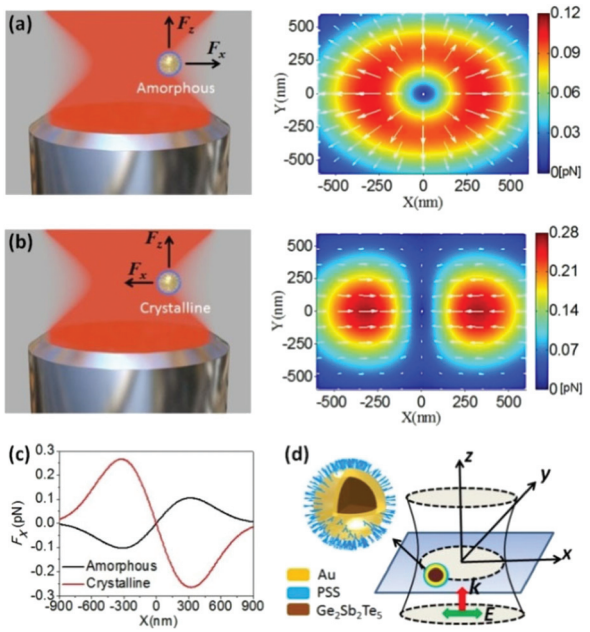

Fig. 1 The configuration of the anomalous lateral force in the phase-change nanoparticle. When the phase-change nanoparticles are at $x = w_0/2$ in a linearly polarized Gaussian wave, they will be pushed forward along the propagation direction of the incident light. The phase-change nanoparticles are shifted in opposite directions for the different structural states of $Ge_2Sb_2Te_5$ by an anomalous lateral force. Schematic diagrams for (a) an amorphous nanoparticle covered by PSS shifted outward from the center of the beam; and (b) a crystalline nanoparticle covered by PSS shifted toward the center of the beam. The right hand columns in (a) and (b) are the corresponding transverse force vector F_x at different positions of the focal plane of the Gaussian beam, where the beam waist of the Gaussian beam is w_0 = 500 nm and the power of the beam is P_0 = 10 mW. Both of the situations are excited at λ = 640 nm. The white arrows and colors present the direction and magnitude of the optical forces F_x in the focal plane, respectively. (c) F_x on the phase-change nanoparticles bound with PSS along the x-axis for both amorphous and crystalline states at λ = 640 nm and P_0 = 10 mW. (d) The scheme of the phase-change nanoparticles in the focal plane of the Gaussian beam. The structure of the phase-change nanoparticle is shown in the inset, where the radius of the $Ge_2Sb_2Te_5$ core is R_{PCM} = 70 nm, the Au shell thickness is T_{Au} = 20 nm and the thickness of the PSS layer is 1 nm. The wave vector and polarization are indicated by the red and green arrows.

Importantly, the nanoparticles undergo Brownian motion with a thermal energy of k_BT, where k_B is the Boltzmann constant and T is the absolute temperature of the environment (T = 300 K for water).[49] To evaluate the stability of the trapping of the phase-change nanoparticles, here the total lateral force F_x, expressed as eqn (11), exerted on the different state nanoparticles at various positions in the focal plane of the Gaussian beam (z = 0 plane) are investigated. The right hand column of Fig. 1(a) shows the vector picture of F_x for the amorphous nanoparticle excited at λ = 640 nm, where the white arrows and colors show the direction and magnitude of F_x in the focal plane, respectively. Here F_x pushes the particle away from the beam center, since the DQ-FR is switched "off" at λ = 640 nm and the net total lateral force F_x is mainly dominated by the lateral scattering force ${}^{S}F_x$ (see detailed discussions in Fig. 2(c)).

By changing the state of the $Ge_2Sb_2Te_5$ core from amorphous to crystalline, the right hand column of Fig. 1(b) shows that F_x drags the crystalline particle towards the Gaussian beam center indicated by the white arrows, because the DQ-FR is switched "on" leading to an attractive F_x, which is also further explained in Fig. 2(d).Interestingly, here the DQ-FR gives rise to a non-conservative force field, resulting in a larger lateral force along the x-axis compared to the one along the y-axis. This is very different with the conservative gradient force (F_{grad}) in conventional optical manipulation. This is because the non-conservative F_x acting on the crystalline particle is caused by Fano interference excited at higher plasmon modes, whereas the F_{grad} mainly consists of the broad dipole resonance, which is independent of the higher order plasmon modes.

We then studied the total lateral force F_x on the phase-change particle along the x-axis (y = 0, z = 0) at different states as shown in Fig. 1(c). Here, we define the sign of F_x as negative (positive) when the direction of F_x (*i.e.*, the white arrow) points to the $-x$ ($+x$) axis. The numerical investigation has revealed that the F_x distribution takes on a sinusoidal profile. For the amorphous particle, F_x points outward from the center of the beam, meaning that the particle is pushed away from the beam center. It also shows that the value of F_x obtains a maximum value at $x = \pm 325$ nm and decreases gradually to 0 at x = 0 and ±900 nm. Upon the state transition to crystalline, the sign of F_x is reversed accordingly. At any location, F_x points toward the center of the beam, enabling the particle to be bonded to the beam axis. Notably, the absolute value of F_x on the crystalline particle is stronger than that on the amorphous particle, indicating an enhancement of F_x in the DQ-FR.

The real and imaginary parts (*i.e.*, $\varepsilon_1(\omega)$ and $\varepsilon_2(\omega)$ respectively) of the dielectric function for the different states of

Published on 05 February 2016. Downloaded by National University of Singapore on 12/05/2016 03:40:10.

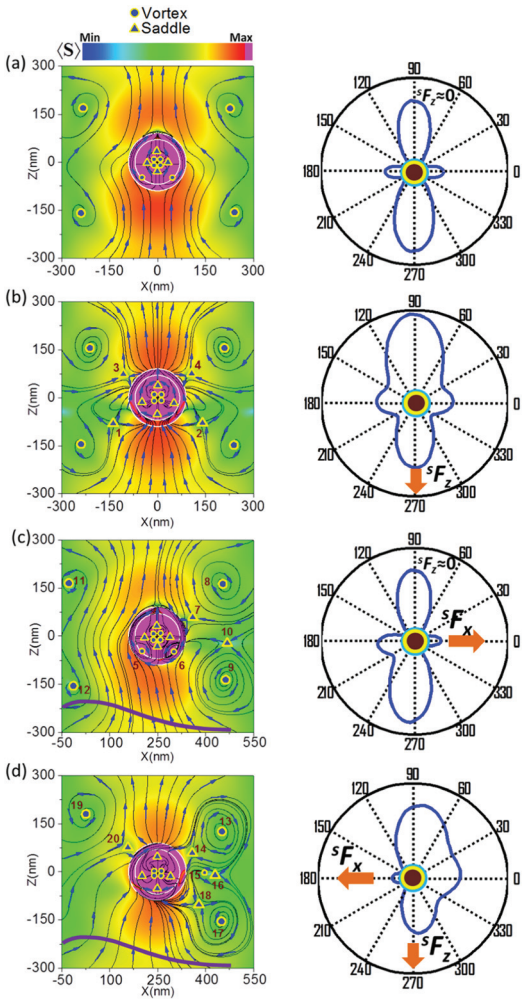

Fig. 2 The intensity distribution and field lines of the Poynting vector **S** for (a) an amorphous nanoparticle and (b) a crystalline nanoparticle positioned at centre of the Gaussian beam; and (c) an amorphous nanoparticle and (d) a crystalline nanoparticle positioned at the half waist of the Gaussian beam. All the situations are excited at 640 nm. The right hand columns in (a), (b), (c) and (d) are the corresponding scattering diagrams in the x–z plane. The brown arrows represent the scattering forces along both the z-axis ($^{S}F_z$) and the x-axis ($^{S}F_x$), which are calculated using eqn (14) and (15) given in the Methods section.

$Ge_2Sb_2Te_5$ were obtained from the published Fourier transform infrared spectroscopy data.[45] A pronounced change in the dielectric function is achieved during the reversible structural transformation from amorphous to crystalline in the visible region (see Fig. S4(a) in ESI S3†). These very different optical properties are realistic and well known but they have predominantly been applied to data storage applications. It should be mentioned that the reversible phase transition in $Ge_2Sb_2Te_5$ is highly repeatable and more than a billion cycles have been experimentally demonstrated in data storage devices. With these unique properties, the Ge–Sb–Te system is of great interest for not only ultrafast data storage but also optical switching and tunable photonic devices.[50] The switchable feature of the DQ-FR of the core–shell particle is associated with the phase change of the $Ge_2Sb_2Te_5$ core medium. The reversible change of the structural states of the $Ge_2Sb_2Te_5$ can be obtained using alternating irradiation of a femtosecond pulsed laser for amorphization and a continuous wave laser for crystallization.

2.2 Near-field singularities and far-field scattering for the $Ge_2Sb_2Te_5$ nanoparticle under a Gaussian beam

The Fano interference-optical lateral force originates from the coupling of the localized surface plasmon and incident wave. The near-field flux can be reversed by tuning the resonant frequency of the FR to switch the direction of the total lateral force. To explore the relation between the near-field singular points and the total lateral force F_x, we show two typical situations: (i) the $Ge_2Sb_2Te_5$ nanoparticle is positioned at the center of the Gaussian beam (x = 0 nm); and (ii) the $Ge_2Sb_2Te_5$ nanoparticle is placed off-axis in a Gaussian beam ($x = w_0/2$ = 250 nm) for both the amorphous and crystalline state. This system consists of vortex and saddle singular points, where the vortex-saddle pairs can control the direction of the energy flowing around them.[43,44] In the left hand column of Fig. 2, we present the near-field singularity distributions and streamlines of **S** in the x–z plane, which clearly expose the scattered energy maps. The color scale and blue arrows are the logarithmic modulus and directions of **S**, respectively. The white circles represent the core–shell particle. The streamlines (shown by black solid lines) follow the solution of a differential equation: $\frac{dr}{d\varphi} = r\frac{\langle S\rangle_r}{\langle S\rangle_\varphi}$, where $\langle S\rangle_r$ and $\langle S\rangle_\phi$ are the components of $\langle \mathbf{S}\rangle$ in polar coordinates.[51] Meanwhile in order to validate the near-field interference as the origin of the directed emission, far-field scattering diagrams are shown in the right hand column of Fig. 2 accordingly.

Fig. 2a shows **S** around the amorphous nanoparticle illuminated by the Gaussian incidence at λ = 640 nm. The particle is placed at x = 0 nm and **S** is expressed by eqn (9) in the Methods section. As can be seen, the scattering of particles may divert the incident **S** away from the propagation direction. Therefore, the momentum of the incident light is larger than that of the transmitted one owing to a considerable amount of scattered light in the backward direction.[52] According to momentum conservation, the backward scattering will lead to a forward total longitudinal force (F_z) exerted on the particle along the direction of the incident light. The F_z consists of the Fano interference-induced longitudinal force $^{S}F_z$ ($^{\mathrm{Fano}}F_z$) that is proportional to the cross-section difference between the downward and upward scattering: $W_{\mathrm{down}} - W_{\mathrm{up}}$. The downward and upward scattering cross-sections are defined as $W_{\mathrm{down}} \approx |3a_1 - 5a_2|^2$, $W_{\mathrm{up}} \approx |3a_1 + 5a_2|^2$, where a_1 and a_2 are Mie scattering coefficients related to the dipole and quadrupole mode, respectively. This shows that $^{S}F_z$ contains the coupling term a_1a_2, representing the contribution from the Fano interference between the dipole and the quadrupole.[37] For the amorphous particle sitting in the center of the incident beam, a symmetric far-field distribution is observed as shown in the right hand

 This journal is © The Royal Society of Chemistry 2016

Published on 05 February 2016. Downloaded by National University of Singapore on 12/05/2016 03:40:10.

column of Fig. 2(a). The magnitude of the scattered field in the upward direction is comparable with that of the incident field, and thus comes up with a zero ${}^{S}F_z$. It is because the DQ-FR is switched "off" at λ = 640 nm for the amorphous nanoparticle whose DQ-FR wavelength is λ = 680 nm (see Fig. 3(b)). This means that the quadrupole mode can be ignored ($a_2 = 0$) and the dipolar resonance dominates the scattered energy flowing around the amorphous nanoparticle at λ = 640 nm. It provides a longitudinally symmetric distribution of the far-field scattering that results in a zero net ${}^{S}F_z$. Here it should be noted that, although ${}^{S}F_z$ as defined in eqn (14) is close to zero, F_z calculated using eqn (11) is still a forward pushing force owing to momentum conservation.

As the state of $Ge_2Sb_2Te_5$ transitions from amorphous to crystalline as shown in Fig. 2(b), four saddle-vortex pairs appear close to the particle at λ = 640 nm and redirect the central energy channel through the particle. For example, part of the incident beam passes through the saddle points in the input of the particle (marked 1 and 2), comes back to the beam center and travels along the propagation direction; moreover, the saddle points in the output (marked 3 and 4) also "grab" the light from the surroundings and bring it towards the transmitted beam center. This will increase the momentum of the transmitted light and in turn reduce the difference between the incident and transmitted momentum. Hence, it may prompt a smaller upward total pushing force F_z compared to in the amorphous case. Nevertheless, the far-field scattering in Fig. 2(b) shows that ${}^{S}F_z$ is a downward scattering force. This is because the excitation of the quadrupole resonance enables a DQ-FR at λ = 640 nm for the crystalline particle. It provides a larger W_{up} than W_{down}, which leads to a net downward ${}^{S}F_z$ containing the coupling term a_1a_2. In other words, the downward ${}^{S}F_z$ acting on the crystalline particle at λ = 640 nm is mainly dominated by the DQ-FR.

Very recently, a remarkable study has demonstrated that under a normal zeroth-order Bessel incidence, a metallic nanoparticle at its FR possesses an asymmetric scattering diagram, where the forward scattering is much stronger than the backward scattering.[53] This leads to a net longitudinal backward optical scattering force. Such a multipolar FR and the induced negative longitudinal scattering force are demonstrated for both homogeneous and hollow metallic particles and thus can be universal for other nanostructures exhibiting FR. Here, the Fano interference-induced longitudinal scattering force ${}^{S}F_z$ exerted to the phase-change sphere follows the same original physics as in ref. 53 and hence is negative when the DQ-FR is excited.

Moreover, it has been shown that the distribution of singular points and energy flows are laterally symmetric when the particle is placed at x = 0 nm for both the amorphous and crystalline spheres. The centrally positioned nanoparticle scatters the same amount of light to the left ($-x$) and to the right ($+x$) and thus light cannot push it sideways. Therefore in the transverse direction, both the total lateral optical force F_x and the Fano interference-induced lateral force ${}^{S}F_x$ (${}^{Fano}F_x$) are zero.

However, the nanoparticle experiences a total lateral optical force F_x as expressed in eqn (13) when the particle is placed at $x = w_0/2$ in the Gaussian beam. To see how this happens, we first present **S** for the amorphous nanoparticle at λ = 640 nm. Fig. 2c shows that the energy flow is asymmetrically distributed: the energy towards the left exceeds the one towards the right; this leads to a net F_x along the $+x$ direction *i.e.*, $F_x > 0$ (see the cyan solid line in Fig. 3(b)). Here, two vortex points (marked 5 and 6) appear at the interface between the $Ge_2Sb_2Te_5$ core and Au shell. The localized surface plasmons interfere constructively with the incident wave, making a loop around the vortex points 5 and 6 and propagating through the surface of the particle along the same direction as the incident light. Particularly, the light passing through the right hand surface can be transmitted into the surrounding environment through the saddle (marked 7), circles around the vortex (marked 8) and comes back to the saddle 7. Although the vortex (marked 9) and saddle (marked 10) form a vortex-saddle pair to guide the light from the surroundings towards the right of sphere, it does not significantly enhance the light energy since this saddle-vortex pair does not appear in the vicinity of the particle.

On the left side of the sphere, two vortices (marked 11 and 12) occur but they are also far away from the particle. Therefore, the incident Gaussian beam does not interact considerably with the particle and basically maintains its profile after transmitting through the particle. Since the left side of the sphere is closer to the central axis of the Gaussian beam, the energy on the left side is higher than the right, exerting a rightward lateral force on the particle ($F_x > 0$).

In the right hand column of Fig. 2(c), we present an asymmetric far-field distribution for the amorphous particle accordingly. It shows that the scattering towards the left significantly surpasses the scattering towards the right hence leading to a rightward ${}^{S}F_x$ (${}^{S}F_x > 0$) calculated using eqn (15) in the Methods section. Here, the ${}^{S}F_x$ pushing the particle away from the beam center can be larger than the gradient force F_{grad} in conventional optical tweezers, where the F_{grad} drags the particle to the beam center. Thus, the total lateral force F_x is positive.

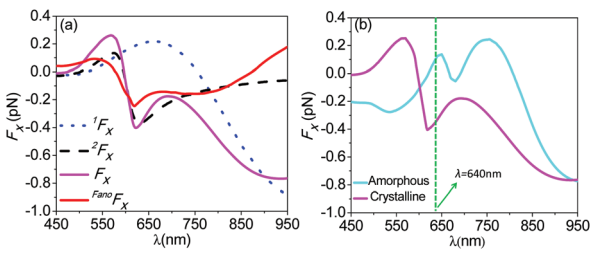

Fig. 3 (a) Total lateral force F_x exerted on the phase-change nanoparticle with a crystalline $Ge_2Sb_2Te_5$ core (radius: R_{PCM} = 70 nm) and a gold shell (thickness: T_{Au} = 20 nm) bonded to PSS, as a function of the wavelength of the incident Gaussian beam. (b) F_x for both the crystalline nanoparticle shown by the pink solid line and the amorphous nanoparticle shown by the cyan solid line. The nanoparticles are both bonded to PSS in the water environment.

Published on 05 February 2016. Downloaded by National University of Singapore on 12/05/2016 03:40:10.

For the crystalline particle at $x = w_0/2$, Fig. 2(d) shows that the energy towards the right surpasses the energy towards the left hence switching the direction of F_x, *i.e.*, $F_x < 0$ (see the pink solid line in Fig. 3(b)). This is because the phase transition of the $Ge_2Sb_2Te_5$ core medium will tune the DQ-FR wavelength. Namely, the phase transition to crystalline switches "on" the DQ-FR around $\lambda = 640$ nm and the F_x mainly consists of the DQ-FR.

Meanwhile the singular points on the interface between the $Ge_2Sb_2Te_5$ core and Au shell disappear, however new singular points are excited in the surrounding environment and move towards the crystalline particle. On the right hand side of the particle, three vortex-saddle pairs are created and marked as 13 (vortex)–14 (saddle), 15 (vortex)–16 (saddle), and 17 (vortex)–18 (saddle). These vortex-saddle pairs reveal the dramatic change in energy flow around them, such that the saddle points "grab" the light from the surroundings and the vortex points "store" the light within the whirlpool region. As a result, these singular points can attract, lead, and converge the energy flow into the right edge of the particle. This is akin to the phenomenon of a non-diffracting tractor beam exerting pulling forces on dielectric particles by continuously dragging them towards the beam sources, where the particle captures energy from the surrounding whirlpools to obtain a pulling optical force hence moving towards the beam source.[52] Meanwhile a vortex (19)–saddle (20) pair can also guide the energy flow to the left of particle, but the strength is much weaker owing to its longer distance from the particle. Thus, the right hand side energy is more pronounced than the left, leading to a leftward total lateral force ($F_x < 0$).

Accordingly, far-field scattering reveals an asymmetric distribution. The sign of the lateral scattering force (${}^{S}F_x$) exerted on the particle can be changed from rightward (${}^{S}F_x > 0$) to leftward (${}^{S}F_x < 0$) by changing the state of $Ge_2Sb_2Te_5$ from amorphous to crystalline. Particularly, this lateral scattering force (${}^{S}F_x$) induced by the DQ-FR can drag the crystalline particle to the beam center, having similar behavior to F_{grad}. Therefore, F_x acting on the crystalline particle is negative. Interestingly, the phase transition of the $Ge_2Sb_2Te_5$ between the amorphous and crystalline state also changes ${}^{S}F_z$ from 0 to backwards, showing the potential of manipulating the phase-change nanoparticles in the longitudinal direction.

These energy patterns show that the phase-change nanoparticle under inhomogeneous incident light produces asymmetrically transverse scattering and thus a total lateral force F_x. The sign of F_x exerted on the particle can be swapped by reversibly switching the state of $Ge_2Sb_2Te_5$ between the amorphous and crystalline state. Notably for the phase-changed particle positioned off-axis in the Gaussian beam, F_z will push it in the direction of the incident wave independent of the state of the $Ge_2Sb_2Te_5$.

2.3 Lateral optical force induced by DQ-FRs

The Maxwell stress tensor method is used to calculate the lateral optical force exerted on the phase-change nanoparticle (see Methods). For example, taking the crystalline nanoparticle, Fig. 3(a) shows that the lateral optical force acting on the particle is contributed to by the different plasmon modes. The expression of the scattering electrical field is shown in eqn (7) in the Methods section, where n represents the order of the different plasmon modes.[54] In the dipole approximation ($n = 1$), the time-averaged dipolar lateral force (or gradient force) ${}^{1}F_x$ exerted on the nanoparticle by the Gaussian wave is given by eqn (11).

As presented by the blue dotted line in Fig. 3(a), ${}^{1}F_x$ is evident and gradually changes over a wide range of wavelengths from 450 to 950 nm. The crystalline nanoparticle experiences a repulsive dipolar lateral force (${}^{1}F_x > 0$) over the blue side of the dipolar resonant wavelength of $\lambda_{dipole} = 755$ nm (the wavelength where ${}^{1}F_x = 0$). The lateral quadrupolar force ${}^{2}F_x$ ($n = 2$) is shown by the black dashed line, where ${}^{2}F_x$ repels the crystalline particle away from the high intensity region (${}^{2}F_x > 0$) on the blue side of the quadrupolar resonance wavelength of $\lambda_{quad} = 595$ nm (the wavelength where ${}^{2}F_x = 0$); For $\lambda > \lambda_{quad}$, ${}^{2}F_x$ changes steeply from repulsive to attractive (${}^{2}F_x < 0$) to drag the particle towards the region of the highest intensity. As shown by the pink solid line, the total lateral optical force F_x ($n = 12$) exhibits a profoundly asymmetric resonance dip ($F_x = -0.41$ pN) around the wavelength of 640 nm, indicating a strongly attractive force. It can be seen that this all mode lateral force F_x is significantly different to the scalar summation of the dipolar lateral force ${}^{1}F_x$ and the quadrupolar lateral force ${}^{2}F_x$. This is because F_x contains the interaction term between the dipolar and quadrupolar resonances that gives rise to the Fano interference force ${}^{Fano}F_x$ (${}^{S}F_x$). Namely, F_x can be expressed by $F_x = {}^{1}F_x + {}^{2}F_x + {}^{Fano}F_x$,[37] where ${}^{Fano}F_x$ is demonstrated by the red solid line in Fig. 3(a). The value of the Fano interference force is ${}^{Fano}F_x = -0.2$ pN at $\lambda = 640$ nm.

Fig. 3b shows the comparison of F_x between the amorphous and crystalline nanoparticles located at $x = w_0/2$ in the focal plane of a Gaussian pulse. Changing the phase of the $Ge_2Sb_2Te_5$ from amorphous to crystalline spectrally tunes the DQ-FR and thus blue-shifts the dip of F_x from 680 to 620 nm. It is important to note that F_x takes an opposite sign for the amorphous nanoparticle ($F_x = 0.14$ pN) and the crystalline nanoparticle ($F_x = -0.34$ pN) at $\lambda = 640$ nm. Thanks to the different signs of F_x, one can distinguish the $Ge_2Sb_2Te_5$ nanoparticles with different structural states. Interestingly, reversibly switching the state of $Ge_2Sb_2Te_5$ between amorphous and crystalline can swap the sign of F_x exerted on the nanoparticle hence alternatively manipulating the particle in the reversible direction. More importantly, many research efforts have been made to reduce the phase change transition time of Ge–Sb–Te phase changed materials, showing the possibility of achieving a time faster than 100 ns.[55] In particular, an optical method has been presented where the crystallization time of $Ge_2Sb_2Te_5$ under focused laser irradiation (incident light power is 8 mW) is as short as 10 ns.[56] This research paves the way to the ultrafast optical sorting of $Ge_2Sb_2Te_5$ nanoparticles which may bring a new method to the field of fast real-time bio-sample detection.

The excitation of higher order multipolar modes ($n \geq 3$) can also interfere with the broad dipolar mode and generate

 This journal is © The Royal Society of Chemistry 2016

Published on 05 February 2016. Downloaded by National University of Singapore on 12/05/2016 03:40:10.

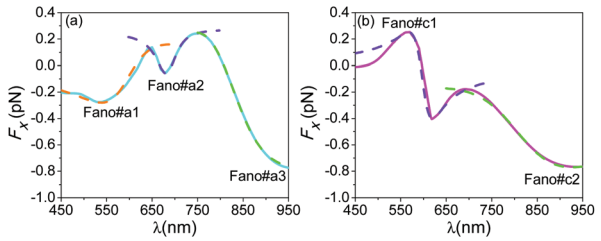

Fig. 4 Fano fitting of the F_x spectra for the (a) amorphous particle, and (b) crystalline particle.

higher order FR, leading to a higher order interference Fano force (*i.e.* a Fano force induced by a quadrupole–octupole interaction).[23] However, here one can neglect the effect of the higher order modes ($n \geq 3$) on the total lateral force F_x. For example, octupole resonance is relatively poor owing to the small size of the nanoparticles. Thus, high-order Fano induced forces caused by the interference between the quadrupole and the octupole are not pronounced in the spectra of F_x ($n = 12$) and $n = 2$ is enough for the convergence.

In Fig. 4, we fit the spectra of F_x exerted on both the amorphous and crystalline particles, using the FR line-shape given in eqn (1).[21–23]

$$I_{\text{Fano}} = I_0 \frac{1}{1+\Gamma^2} \frac{(\Gamma\gamma + \omega - \omega_0)}{(\omega - \omega_0)^2 + \gamma^2} + I_b \quad (1)$$

Here, ω_0 is the resonant frequency, γ is the line-width of the autoionized states (the resonant line-width at half maximum, FWHM) of the resonant modes, Γ is the so-called Fano factor (asymmetry parameter) that determines the degree of asymmetry, I_0 is the intensity of resonance, and I_b is a background value. The F_x curve for each state possesses several resonant peaks in each curve. With the parameters shown in Table 1, F_x fitted using eqn (1) approximately reproduces our calculation data for the amorphous particle shown in Fig. 4(a) and the crystalline particle shown in Fig. 4(b). It can be found that the Fano formula mostly matches the calculation data around the resonant modes.

Note that conventional optical tweezers suffer difficulties in stably trapping small nanoparticles possessing sizes of the order of nanometers, since the radiation force dramatically decreases as the size of the molecule becomes smaller and the pressure is too small to overcome the thermal fluctuations.[57] As a result, optical trapping of smaller particles needs a high incident light power. As shown in Fig. 3, the DQ-FR induced lateral optical force acting on the nanoparticles has a great advantage in terms of the incident light power: a significant attractive (negative) lateral force can be achieved around the DQ-FR wavelength with a low incident power (P_0 = 10 mW), owing to the electromagnetic enhancement effect of the DQ-FR.

Due to the difference in the absorptivity of $Ge_2Sb_2Te_5$ materials in the crystalline and amorphous states, one may have variations in the optical parameters relating to different temperatures of these phase-change particles. However, in our case a difference in the absorption cross section (C_{abs}) of the particles in the amorphous and crystalline states is not large at around λ = 640 nm, where $C_{\text{abs}} = 2.2 \times 10^{-13}$ m^2 for the amorphous state and $C_{\text{abs}} = 1.4 \times 10^{-13}$ m^2 for the crystalline state (see ESI Fig. S1†) This indicates a small difference in the absorptivity of the particles in the amorphous and crystalline states. Moreover, the phase-change nanoparticles are manipulated using a Gaussian pulse with a very low power intensity (~10 mW μm^{-2}) and have a cooling effect owing to the convection in the aqueous environment. Therefore, herein optical heating may not significantly disturb the optical parameters of the phase-change particles. Calculations of C_{abs} for the amorphous and crystalline nanoparticles are presented in ESI S1.†

Furthermore, for the nanoparticle with random Brownian motion in the aqueous environment, it is necessary to analyze its stability.[60,61] Therefore, dynamic simulations are performed, as shown in ESI S3 and Movies,† which show time sequences of the movements of the phase-change spheres (R_{PCM} = 70 nm, T_{Au} = 20 nm) for the amorphous and crystalline states in the focal plane of the Gaussian beam (z = 0 plane).

Table 1 Parameters used in the FR line-shape to fit the F_x spectra for both the amorphous and crystalline nanoparticles

Label	ω_0	γ	Γ	I_0	I_b
Fano#a1	3.15×10^{15}	3.90×10^{14}	−0.90	0.44	−0.28
Fano#a2	2.75×10^{15}	1.10×10^{13}	−0.15	0.33	−0.06
Fano#a3	2.28×10^{15}	3.00×10^{14}	1.20	1.02	−0.77
Fano#c1	3.14×10^{15}	1.35×10^{14}	0.75	0.65	−0.40
Fano#c2	2.23×10^{15}	3.90×10^{14}	0.50	0.60	−0.77

3. Conclusions

In summary, the concept of ultrafast reversible sorting of phase-change nanoparticles has been illustrated by manipulating the dipole–quadrupole Fano interference lateral force on the particles. We have shown that, under inhomogeneous excitation, the Fano interference between the dipolar and quadrupolar modes can provide a lateral asymmetric energy distribution thus exerting a sideways force on the particle. This Fano interference force can laterally push the nanoparticles with different structural states of $Ge_2Sb_2Te_5$ in opposite directions. Furthermore, we explore the fundamental mechanism of the reversal of the DQ-FR induced lateral force using singular optics that is based on molding the optical power flow through singular points inside and around the phase-change nanoparticles. Importantly, the short phase transition time of $Ge_2Sb_2Te_5$ between the amorphous and crystalline states (<10 ns) allows us to achieve an ultrafast sorting of the phase-change nanoparticles. We also suggest that this unique scheme may be used to sort small biomolecules such as PSS. Flexible control of the direction and magnitude of the lateral optical force paves the way for the observation of the collective phenomena of nanoparticles, and may be harnessed to realize

Published on 05 February 2016. Downloaded by National University of Singapore on 12/05/2016 03:40:10.

a new generation of active and self-adaptive nano-optomechanical systems based on phase-change materials.

4. Methods

In terms of spherical vector wave functions (SVWFs), the electric field ($\mathbf{E}^{\mathrm{i}}$) and magnetic field ($\mathbf{H}^{\mathrm{i}}$) of the incident Gaussian beam can be expanded to the particle coordinate system by introducing the corresponding off-axis Gaussian expansion coefficients ${}^{\mathrm{G}}C_{nm1}$ and ${}^{\mathrm{G}}C_{nm2}$ [58]

$$\mathbf{E}^{\mathrm{i}} = E_0 \sum_{n=1}^{\infty} \sum_{m=-n}^{n} \left[{}^{\mathrm{G}}C_{nm1} \mathbf{M}_{mn}{}^{1}(\mathbf{r}, k_0) + {}^{\mathrm{G}}C_{nm2} \mathbf{N}_{mn}{}^{1}(\mathbf{r}, k_0) \right] \quad (2)$$

$$\mathbf{H}^{\mathrm{i}} = E_0 \frac{k_0}{i\omega\mu_0} \sum_{n=1}^{\infty} \sum_{m=-n}^{n} \left[{}^{\mathrm{G}}C_{nm1} \mathbf{N}_{mn}{}^{1}(\mathbf{r}, k_0) + {}^{\mathrm{G}}C_{nm2} \mathbf{M}_{mn}{}^{1}(\mathbf{r}, k_0) \right] \quad (3)$$

where $k_0 = 2\pi/\lambda$ and λ is the wavelength of the incident light in the environmental medium, μ_0 is the permeability of the environmental medium, and E_0 is the magnitude of the electric field at the beam waist center. $n \in [1,\infty]$ are the multipole orders and $m \in [-n,n]$ are the angular numbers. $\mathbf{M}_{mn}{}^{(l)}$ and $\mathbf{N}_{mn}{}^{(l)}$ are the SVWFs, expressed as

$$\mathbf{M}_{mn}{}^{(l)}(kr,\theta,\phi) = z_n{}^{(l)}(kr) \times \left[im \frac{P_n{}^{m}(\cos\theta)}{\sin\theta} \mathrm{e}^{im\phi}\hat{\theta} - \frac{\mathrm{d}P_n{}^{m}(\cos\theta)}{\mathrm{d}\theta} \mathrm{e}^{im\phi}\hat{\phi} \right] \quad (4)$$

$$\mathbf{N}_{mn}{}^{(l)}(kr,\theta,\phi) = n(n+1)\frac{z_n{}^{(l)}(kr)}{kr} P_n{}^{m}(\cos\theta)\mathrm{e}^{im\phi}\hat{r} + \frac{1}{kr}\frac{\mathrm{d}(rz_n{}^{(l)}(kr))}{\mathrm{d}r}\left[\frac{\mathrm{d}P_n{}^{m}(\cos\theta)}{\mathrm{d}\theta}\hat{\theta} + im\frac{P_n{}^{m}(\cos\theta)}{\sin\theta}\hat{\phi} \right]\mathrm{e}^{im\phi} \quad (5)$$

where $z_n{}^{(l)}$ stands for a proper kind of spherical Bessel function: the first kind j_n, the second kind y_n, or the third kind $h_n{}^{(1)}$ and $h_n{}^{(2)}$, with l = 1, 2, 3, or 4, respectively; $P_n^m(\cos\theta)$ is the associated Legendre polynomial function of the first kind and is defined as[54]

$$P_n^m(\cos\theta) = (-1)^m(\sin\theta)^m \frac{d^m P_n(\cos\theta)}{[d(\cos\theta)]^m} \quad (6)$$

where $P_n(\cos\theta)$ is the Legendre polynomial function of order n.

In particular, the expansion coefficients ${}^{\mathrm{G}}C_{nm1}$ and ${}^{\mathrm{G}}C_{nm2}$ can be expressed in terms of so-called beam shaped coefficients (BSC) $g_{n,\mathrm{TE}}{}^{m}$ and $g_{n,\mathrm{TM}}{}^{m}$.[54,59] The scattering electric field ($\mathbf{E}^{\mathrm{s}}$) and magnetic field ($\mathbf{H}^{\mathrm{s}}$) can be expressed as

$$\mathbf{E}^{\mathrm{s}} = E_0 \sum_{n=1}^{\infty} \sum_{m=-n}^{n} \left[b_{nm} \mathbf{M}_{mn}{}^{3}(\mathbf{r}, k_0) + a_{nm} \mathbf{N}_{mn}{}^{3}(\mathbf{r}, k_0) \right] \quad (7)$$

$$\mathbf{H}^{\mathrm{s}} = E_0 \frac{k_0}{i\omega\mu_0} \sum_{n=1}^{\infty} \sum_{m=-n}^{n} \left[b_{nm} \mathbf{N}_{mn}{}^{3}(\mathbf{r}, k_0) + a_{nm} \mathbf{M}_{mn}{}^{3}(\mathbf{r}, k_0) \right] \quad (8)$$

where a_{nm} and b_{nm} are the expansion coefficients of Mie scattering that can be defined by $a_{nm} = a_n g_{n,\mathrm{TM}}{}^{m}$ and $b_{nm} = b_n g_{n,\mathrm{TE}}{}^{m}$, a_n and b_n is the usual scattering coefficient of the Lorenz-Mie theory.[54]

The energy flow, namely the time-averaged Poynting vector due to the all field is calculated by

$$\langle \mathbf{S} \rangle = \frac{1}{2}\mathrm{Re}(\mathbf{E} \times \mathbf{H}^*) \quad (9)$$

where Re denotes the real part, and the superscript * denotes the complex conjugate. The fields $\mathbf{E}$ and $\mathbf{H}$ in eqn (9) are the total fields given by

$$\mathbf{E} = \mathbf{E}^{\mathrm{i}} + \mathbf{E}^{\mathrm{s}}, \mathbf{H} = \mathbf{H}^{\mathrm{i}} + \mathbf{H}^{\mathrm{s}} \quad (10)$$

Here, the time-averaged optical force acting on the phase-change nanoparticle under the illumination of an off-axis Gaussian beam is calculated in terms of the surface integration of the Maxwell stress tensor

$$\langle \mathbf{F} \rangle = \oint_{\mathrm{s}} \langle \mathbf{T} \cdot \hat{\mathbf{r}} \rangle \mathrm{d}S_{\mathrm{surface}} \quad (11)$$

where the Maxwell stress tensor $\mathbf{T}$ is given by

$$\mathbf{T} = \varepsilon\mathbf{E}\mathbf{E} + \mu\mathbf{H}\mathbf{H} - 1/2(\varepsilon E^2 + \mu H^2)\delta \quad (12)$$

The transverse component of $\langle \mathbf{F} \rangle$ can be defined in terms of the basis vector transformation:

$$F_x = \int_0^{2\pi}\int_0^{\pi} T_{\mathrm{r}} R^2 \sin^2\theta \cos\varphi \, d\theta d\varphi \quad (13)$$

where $T_{\mathrm{r}} = \frac{1}{2}[\varepsilon(E_{\mathrm{r}}E_{\mathrm{r}}{}^* - E_\theta E_\theta{}^* - E_\varphi E_\varphi{}^*) + \mu(H_{\mathrm{r}}H_{\mathrm{r}}{}^* - H_\theta H_\theta{}^* - H_\varphi H_\varphi{}^*)]$, R is the radius of the integrating sphere, and ε and μ are the permittivity and permeability of the surrounding medium, respectively.

The integration for the optical force in eqn (11) is evaluated over the outer surface S_{surface} enclosing the nanoparticle, while $\hat{\mathbf{r}}$ and $\mathrm{d}S_{\mathrm{surface}}$ are, respectively, the local outward normal unit vector and the area element of the surface S_{surface}, and δ is a unit matrix.

The scattering force $\langle {}^{s}\mathbf{F} \rangle$ containing the coupling term between different plasmon modes can be expressed as

$$\langle {}^{\mathrm{s}}\mathbf{F} \rangle = \oint_{\mathrm{s}} \langle {}^{\mathrm{s}}\mathbf{T} \cdot \hat{\mathbf{r}} \rangle \mathrm{d}S_{\mathrm{surface}} = \oint_{\mathrm{s}} \left\langle \varepsilon^{\mathrm{s}} E_{\mathrm{r}}{}^{\mathrm{s}}\mathbf{E} + \mu^{\mathrm{s}} H_{\mathrm{r}}{}^{\mathrm{s}}\mathbf{H} - \frac{1}{2}(\varepsilon^{\mathrm{s}}E^2 + \mu H^2)\hat{\mathbf{r}} \right\rangle \mathrm{d}S_{\mathrm{surface}} \quad (14)$$

where ${}^{\mathrm{s}}\mathbf{T} = \varepsilon^{\mathrm{s}}\mathbf{E}^{\mathrm{s}}\mathbf{E} + \mu^{\mathrm{s}}\mathbf{H}^{\mathrm{s}}\mathbf{H} - \frac{1}{2}(\varepsilon^{\mathrm{s}}E^2 + \mu^{\mathrm{s}}H^2)\delta$.

Under the normal incident off-axis Gaussian beam, the attractive (negative) Fano interference force originating from the transverse component of $\langle {}^{s}\mathbf{F} \rangle$ is able to be used for trapping the nanoparticles. For example, the scattering force exerted on the nanoparticle on the x-axis can be defined in terms of the basis vector transformation:[37]

$${}^{s}F_x = {}^{\mathrm{Fano}}F_x = \int_0^{2\pi}\int_0^{\pi} {}^{\mathrm{s}}T_{\mathrm{r}} R^2 \sin^2\theta \cos\varphi \, d\theta d\varphi \quad (15)$$

 This journal is © The Royal Society of Chemistry 2016

Published on 05 February 2016. Downloaded by National University of Singapore on 12/05/2016 03:40:10.

where ${}^{s}T_{r} = \frac{1}{2}[\varepsilon({}^{s}E_{r}{}^{s}E_{r}{}^{*} - {}^{s}E_{\theta}{}^{s}E_{\theta}{}^{*} - {}^{s}E_{\varphi}{}^{s}E_{\varphi}{}^{*}) + \mu({}^{s}H_{r}{}^{s}H_{r}{}^{*} - {}^{s}H_{\theta}{}^{s}H_{\theta}{}^{*} - {}^{s}H_{\varphi}{}^{s}H_{\varphi}{}^{*})]$ and R is the radius of the integrating sphere. Note that, ${}^{Fano}F_{x}$ consists of the interference term between the adjacent plasmon modes hence giving rise to the Fano interference lateral optical force along the x-axis.

Acknowledgements

This work was supported by National Natural Science Foundation of China (Grant No. 61172059, 51302026, 11504252), International Science & Technology Cooperation Program of China (Grant No.2015DFG12630), Program for Liaoning Excellent Talents in University (Grant No. LJQ2015021) and the Fundamental Research for the Central University (Grant No. DUT14YQ109).

Notes and references

1 T. Shoji, J. Saitoh, N. Kitamura, F. Nagasawa, K. Murakoshi, H. Yamauchi, S. Ito, H. Miyasaka, H. Ishihara and Y. Tsuboi, *J. Am. Chem. Soc.*, 2013, **135**, 6643–6648.
2 V. G. Shvedov, A. V. Rode, Y. V. Izdebskaya, A. S. Desyatnikov, W. Krolikowski and Y. S. Kivshar, *Phys. Rev. Lett.*, 2010, **105**, 118103–118104.
3 H. X. Xu, *Phys. Lett. A*, 2003, **312**, 411–419.
4 J. M. Auñón and M. Nieto-Vesperinas, *J. Opt. Soc. Am. A*, 2014, **31**, 1984.
5 A. S. Urban, C. P. Sol, A. A. Lutich, T. Lohmüller, J. Feldmann and F. Jäckel, *Nanoscale*, 2014, **6**, 4458–4474.
6 T. J. Kippenberg and K. J. Vahala, *Science*, 2008, **321**, 1172–1176.
7 P. T. Rakich, P. Davids and Z. Wang, *Opt. Express*, 2010, **18**, 14439–14453.
8 A. Ashkin, J. M. Dziedzic, J. E. Bjorkholm and S. Chu, *Opt. Lett.*, 1986, **11**, 288–290.
9 D. Zerrouki, J. Baudry, D. Pine, P. Chaikin and J. Bibette, *Nature*, 2008, **455**, 380–382.
10 T. J. Ward and B. A. Baker, *Anal. Chem.*, 2008, **80**, 4363–4372.
11 K. Y. Bliokh, Y. S. Kivshar and F. Nori, *Phys. Rev. Lett.*, 2014, **113**, 033601.
12 Y. Tang and A. E. Cohen, *Phys. Rev. Lett.*, 2010, **104**, 163901.
13 Y. Tang and A. E. Cohen, *Science*, 2011, **332**, 333–336.
14 G. Tkachenko and E. Brasselet, *Phys. Rev. Lett.*, 2013, **111**, 033605.
15 G. Tkachenko and E. Brasselet, *Nat. Commun.*, 2014, **5**, 3577.
16 G. Tkachenko and E. Brasselet, *Nat. Commun.*, 2014, **5**, 4491.
17 S. B. Wang and C. T. Chan, *Nat. Commun.*, 2014, **5**, 3307.
18 F. J. Rodríguez-Fortuño, N. Engheta, A. Martínez and A. V. Zayats, *Nat. Commun.*, 2015, **6**, 8799.
19 H. J. Chen, N. Wang, W. L. Lu, S. Y. Liu and Z. F. Lin, *Phys. Rev. A: Condens. Matter*, 2014, **90**, 043850.
20 H. J. Chen, Y. K. Jiang, N. Wang, W. L. Lu, S. Y. Liu and Z. F. Lin, *Opt. Lett.*, 2015, **40**, 5530.
21 U. Fano, *Phys. Rev.*, 1961, **124**, 1866.
22 A. E. Miroshnichenko, S. Flach and Y. S. Kivshar, *Rev. Mod. Phys.*, 2010, **82**, 2257.
23 B. Luk'yanchuk, N. I. Zheludev, S. A. Maier, N. J. Halas, P. Nordlander, H. Giessen and C. T. Chong, *Nat. Mater.*, 2010, **9**, 707–715.
24 Y. Zhang, Y. R. Zhen, O. Neumann, J. K. Day, P. Nordlander and N. J. Halas, *Nat. Commun.*, 2014, **5**, 4424.
25 F. Lütolf, O. J. F. Martin and B. Gallinet, *Nanoscale*, 2015, **7**, 18179–18187.
26 N. Liu, S. Mukherjee, K. Bao, Y. Li, L. V. Brown, P. Nordlander and N. J. Halas, *ACS Nano*, 2012, **6**, 5482–5488.
27 H. D. Deng, X. Y. Chen, Y. Xu and A. E. Miroshnichenko, *Nanoscale*, 2015, **7**, 20405–20413.
28 K. E. Chong, B. Hopkins, I. Staude, A. E. Miroshnichenko, J. Dominguez, M. Decker, D. N. Neshev, I. Brener and Y. S. Kivshar, *Small*, 2014, **10**, 1985–1990.
29 R. Asadi, Z. Ouyang and M. M. Mohammd, *Nanoscale*, 2015, **7**, 11379–11385.
30 S. P. Zhang, K. Bao, N. J. Halas, H. X. Xu and P. Nordlander, *Nano Lett.*, 2011, **8**, 1657–1663.
31 N. S. King, L. Liu, X. Yang, B. Cerjan, H. O. Everitt, P. Nordlander and N. J. Halas, *ACS Nano*, 2015, **9**, 10628–10636.
32 W. S. Chang, J. B. Lassiter, P. Swanglap, H. Sobhani, S. Khatua, P. Nordlander, N. J. Halas and S. A. Link, *Nano Lett.*, 2012, **12**, 4977–4982.
33 N. Liu, F. F. Wen, Y. Zhao, Y. Wang, P. Nordlander, N. J. Halas and A. Alu, *Nano Lett.*, 2013, **13**, 142–147.
34 M. V. Rybin, P. V. Kapitanova, D. S. Filonov, A. P. Slobozhanyuk, P. A. Belov, Y. S. Kivshar and M. F. Limonov, *Phys. Rev. B: Condens. Matter*, 2013, **88**, 205106–205108.
35 Z. P. Li, T. Shegai, G. Haran and H. X. Xu, *ACS Nano*, 2009, **3**, 637–642.
36 Y. Zhang, F. Wen, Y. R. Zhen, P. Nordlander and N. J. Halas, *Proc. Natl. Acad. Sci. U. S. A.*, 2013, **110**, 9215–9219.
37 Z. Li, S. Zhang, L. Tong, P. Wang, B. Dong and H. Xu, *ACS Nano*, 2013, **8**, 701–708.
38 H. X. Xu, *Phys. Rev. B: Condens. Matter*, 2005, **72**, 073405.
39 J. F. Nye and M. V. Berry, *Proc. R. Soc. London. Ser. A*, 1974, **336**, 165–190.
40 J. Chen, J. Ng, Z. Lin and C. T. Chan, *Nat. Photonics*, 2011, **5**, 531.
41 A. Novitsky, C. W. Qiu and H. Wang, *Phys. Rev. Lett.*, 2011, **107**, 203601.
42 M. I. Tribelsky and B. S. Luk'yanchuk, *Phys. Rev. Lett.*, 2006, **97**, 263902.
43 D. L. Gao, L. Gao, A. Novitsky, H. L. Chen and B. Luk'yanchuk, *Opt. Lett.*, 2015, **40**, 4162–4165.
44 A. Bekshaev, K. Y. Bliokh and M. Soskin, *J. Opt.*, 2011, **13**, 053001.

Published on 05 February 2016. Downloaded by National University of Singapore on 12/05/2016 03:40:10.

45 K. Shportko, S. Kremers, M. Woda, D. Lencer, J. Robertson and M. Wuttig, *Nat. Mater.*, 2008, **7**, 653–658.
46 D. Loke, T. H. Lee, W. J. Wang, L. P. Shi, R. Zhao, Y. C. Yeo, T. C. Chong and S. R. Elliott, *Science*, 2012, **336**, 1566–1569.
47 L. V. Brown, H. Sobhani, J. B. Lassiter, P. Nordlander and N. J. Halas, *ACS Nano*, 2010, **4**, 819–832.
48 P. B. Johnson and R. W. Christy, *Phys. Rev. B: Condens. Matter*, 1972, **6**, 4370.
49 T. Shoji and Y. Tsuboi, *J. Phys. Chem. Lett.*, 2014, **5**, 2957–2967.
50 T. Hira, T. Homma, T. Uchiyama, K. Kuwamura and T. Saiki, *Appl. Phys. Lett.*, 2013, **103**, 241101.
51 B. S. Luk'Yanchuk and V. Ternovsky, *Phys. Rev. B: Condens. Matter*, 2006, **73**, 235432.
52 D. L. Gao, A. Novitsky, T. Zhang, F. C. Cheong, L. Gao, C. T. Lim, B. Luk'yanchuk and C. W. Qiu, *Laser Photonics Rev.*, 2015, **9**, 75–82.
53 H. J. Chen, S. Y. Liu, J. Zi and Z. F. Lin, *ACS Nano*, 2015, **9**, 1926.
54 G. Gouesbet, B. Maheu and G. Grehan, *J. Opt. Soc. Am. A*, 1988, **5**, 1427–1443.
55 F. Xiong, A. D. Liao, D. Estrada and E. Pop, *Science*, 2011, **332**, 568–570.
56 V. Weidenhof, I. Friedrich, S. Ziegler and M. Wuttig, *J. Appl. Phys.*, 2001, **89**, 3168–3176.
57 P. Y. Wu, R. X. Huang, C. Tischer, A. Jonas and E. L. Florin, *Phys. Rev. Lett.*, 2009, **103**, 108101.
58 Z. Li, Z. Wu and Q. C. Shang, *Opt. Express*, 2011, **19**, 16044–16057.
59 F. Onofri, G. Gréhan and G. Gouesbet, *Appl. Opt.*, 1995, **34**, 7113–7124.
60 P. Langevin, *C. R. Acad. Sci.*, 1908, **146**, 530.
61 P. Hansen, Y. Zheng, J. Ryan and L. Hesselink, *Nano Lett.*, 2014, **14**, 2965.

 This journal is © The Royal Society of Chemistry 2016